Aug 24th, 12:00 AM - Aug 25th, 12:00 AM

An Explicit, Dynamic Finite Element Model for the Local Failure of Cold-formed Trapezoidal Sheeting

Hèrm Hofmeyer

Twenty-First International Specialty Conference on Cold-Formed Steel Structures
St. Louis, Missouri, USA, October 24 & 25, 2012

An explicit, dynamic finite element model for the local failure of cold-formed trapezoidal sheeting

H.(Hèrm) Hofmeyer[1]

Abstract

Trapezoidal sheeting, made of cold-formed, thin-walled steel, is widely used for the construction of cladding and roofs. At an interior support, the sheeting is subject to bending moments and a concentrated load, which leads to possible failure followed by two post-failure modes: the yield-arc and yield-eye modes. Until recently, it was not fully understood why a specific post-failure mode occurs and it was suggested that mode-jumping of the compressed sheeting flange may influence the mode occurring. This paper presents new research, in which both the compressed flange in isolation and the sheeting are modeled by using an explicit, dynamic finite element model. First, it is indicated that the mode-jumping phenomenon is not likely to occur for trapezoidal sheeting as used in practice. Secondly, it will be shown that whether the yield-arc or yield-eye post-failure occurs is mainly related to imperfections and the ratio between stresses caused by bending moment and concentrated load. Lastly, a simple yet accurate formula will be derived, which predicts the post-failure mode occurring, thus enabling further investigations into the sheeting's behavior, like moment redistribution and behavior of second and third generation sheeting.

1 Introduction

Trapezoidal sheeting, made of cold-formed, thin-walled steel, is widely used for the construction of cladding and roofs. At an interior support, the sheeting is subject to bending moments and a concentrated load. Either the concentrated load leads to failure by so-called web-crippling [Macd06a, MacD11a, MacD11b, Tsew08a, Zhou07a], or the combination of web-crippling and bending moment may induce failure [Akha04a, Bieg06a, Bieg08a, Chen12a, Guze06a, Heda08a, Lang06a].

---

[1]Associate Professor in Applied Mechanics, Department of the Built Environment, Eindhoven University of Technology, The Netherlands

This latter failure is followed by two possible post-failure modes: the yield-arc and yield-eye post-failure modes.

For first generation sheeting, which is sheeting without stiffeners, the so-called ultimate failure model enables the prediction of the sheeting's ultimate load for combined concentrated load and bending moment, as shown in figure 1 for a sheet-section [Hofm02a]. A sheet-section is a part of the sheeting, consisting of a compressed flange, two webs, and two half tensioned flanges, assumed to represent the behavior of the sheeting itself.

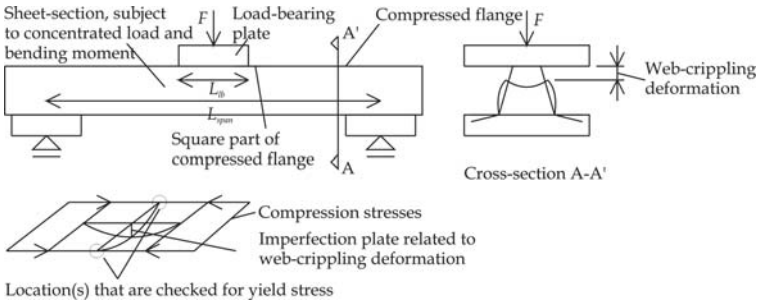

Figure 1, ultimate failure model

The ultimate failure model first determines the elastic indentation of the sheet-section's cross-section (defined as web-crippling deformation) due to the concentrated load using an energy or beam-on-elastic-foundation approach. This web-crippling deformation is then used to calculate the out-of-plane deflection of a square part of the compressed flange. This out-of plane deflection is used as imperfection in Marguerre's plate equations [Marg38a], which can be used to predict the stresses in the square part of the compressed flange. If these stresses reach the yield strength at a specific location, the sheet-section is assumed to fail.

Recently, an alternative for Marguerre's equations within the ultimate failure model was developed, namely the two-strip model. In this model, the nonlinear elastic behavior of a compressed plate is described by dividing the plate into two strips [Bakk06a]. The edge strip behaves linear elastically whereas the centre strip can buckle similar to an Euler column. The initial imperfection and the maximum displacement of the centre strip are scaled to the corresponding values of the real plate using FE-simulations. The nonlinear behavior can be used to predict plate failure by using specific elasto-plastic criteria. The model has been used and discussed in literature [Beda09a, Beda10a, Beda11a, Debo09a,

Than11a]. Because the two-strip model provides insight in the failure behavior of plates without stiffeners and, used within the ultimate failure model, predicts the ultimate load of sheet-sections at least equally correctly as the currently used design rules, it is a candidate for future design rules. However, the question is whether the model is suitable for predicting the behavior of plates with stiffeners. Therefore the nonlinear elastic and failure behavior of plates with stiffeners was studied. Like for plates without stiffeners, this study was carried out with the finite element method because experiments are not accurate enough to control exactly the boundary conditions and initial imperfections of a plate. However, it was shown that even when using a finite element method the boundary conditions cannot be modeled correctly. To explain this, first the standard boundary conditions for a plate without stiffeners as used for the two-strip model are presented (figure 2a). All edges are simply supported, that means $w = 0$. The unloaded edges are free in y-direction (thus the edges are able to "wave" in-plane) or are forced to remain straight but are still able to move along the y-direction. The loaded edges are kept straight and are loaded using displacement control.

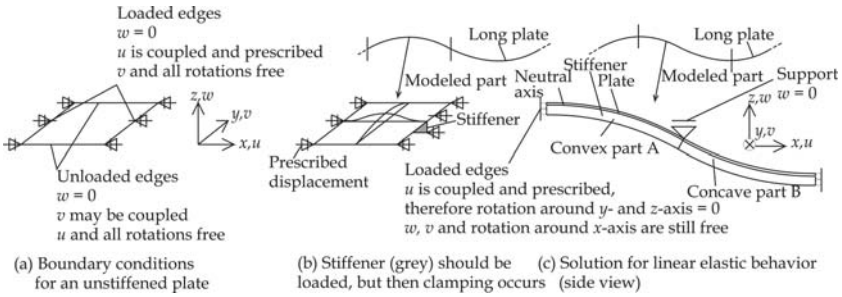

Figure 2, boundary conditions for stiffened plates

If these boundary conditions are used for a plate with an eccentric stiffener and the prescribed displacement along the loaded edge is also applied to the stiffener, the plate bends due to the fact that the load resultant of the prescribed displacement is not in line with the neutral axis, even for a linear elastic simulation, figure 2b. But if only the flat parts of the loaded edges are loaded, the stiffener is not loaded, which does not resembles the situation in practice. A solution for this problem is to model the plate for one half of the convex curved geometry and one half for the concave curved part, figure 2c. Now, the loaded edges of these parts do not rotate in practice and thus no clamping stresses can occur.

However, for an elastic nonlinear simulation, even this solution is not adequate. This because for the convex part (part A in figure 2c) the largest part (neutral axis will be only slightly below the plate surface) of the stiffener is under compression, whereas for the concave part B, the largest part of the stiffener is under tension. This means that for part A the compressed stiffener will amplify the bending of the plate and part B experiences a reduced bending. For this case, it is unlikely that the wave lengths of convex and concave parts are still the same, and the model as shown in figure 2c may show to be erroneous in using the same lengths for both parts. The only solution for these problems is the modeling of the complete compressed flange and applying boundary conditions such that the actions of the webs, the concentrated load and the supports for the sheeting as shown in figure 1 are taken into account.

Modeling the complete compressed flange led, in some situations, to convergence problems in the implicit and static simulations. Therefore explicit and dynamic simulations were used, which revealed that so-called mode-jumping may occur in the sheeting's compressed flange. At this stage, it was realized that first of all the mode-jumping phenomenon should be studied more thoroughly, as its occurrence would undermine the assumptions of the models developed so far, and secondly, the explicit and dynamic simulations, able to handle mode-jumping and other convergence problems, could also be used to investigate the reason why the two specific post-failure modes occur. Namely, until recently, the yield-eye post-failure mode could not be investigated numerically due to convergence problems and these convergence problems could also be linked to mode-jumping. However, it is important to understand why a certain post-failure mode occurs for making design improvements for the sheeting, and for understanding moment redistribution and the behavior of second and third generation sheeting. Therefore, using the dynamic, explicit finite element model, new research was undertaken and the results are presented in this paper.

2 Mode-jumping

Related to which was mentioned above, a difference between the yield-arc and yield-eye post-failure modes could be the fact that before the yield-eye post-failure mode, mode-jumping occurs (which could explain the simulation difficulties for this post-failure mode) whereas this is not the case for the yield-arc post-failure mode. In order to investigate this hypothesis further, in this section, possible mode-jumping phenomena will be investigated for trapezoidal sheeting. This is carried out by modeling the only part possibly prone to mode-jumping (i.e. a part of the compressed flange of the sheeting), in a finite element model such that dynamic behavior (mode-jumping) can be taken into account.

Therefore, explicit dynamic simulations have been used, by means of the program LS-DYNA [Ansy11a].

First of all, an eigen-mode analysis has been carried out as shown in figure 3. The plate shown in figure 3 resembles a part of the compressed flange of trapezoidal sheeting. All edges of the model are simply supported and the model is loaded by a displacement in x-direction of the edge at x = +/- a/2 (thus the stress and strain in the plate are constant initially). In y-direction NE1 (NE1 being a scalar variable to be specified) elements are applied and in x-direction NE1 a/b elements, which will result in square elements for every value of a/b (as long as a/b yields an integer). The element type used to mesh the plate is SHELL181 [Ansy11a]. The calculation of the eigen-modes starts with performing a static analysis with prestress effects. Next, a buckling analysis is performed using the subspace solution method and the first three eigen-modes are extracted. The eigen-modes are saved and will be used in the next analysis as shape for the initial imperfection.

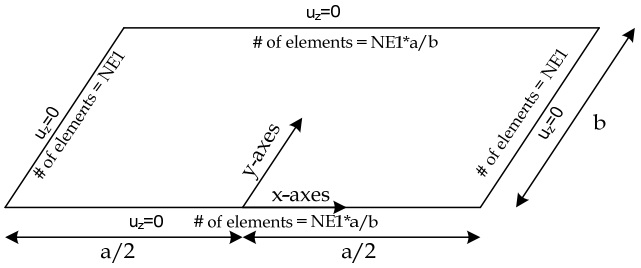

Figure 3, finite element model for buckling analyses of part of compressed flange

After the eigen-mode analysis, an explicit, dynamic finite element analysis was carried out as shown in figure 4. Based on experience [Cour11a], the in-plane displacement of the loaded edges was performed by a linear increasing velocity of the edges (resulting in a quadratic displacement function), the end displacement being reached in 150 ms. Because of the application of the full displacement within 150 ms, a small value of alpha damping (1000), applied to all elements, was useful for damping out oscillations in the reaction forces without compromising the static behavior of the structure too much [Cour11a]. For the material, an isotropic elastic material model was used, with ρ = 7.83E-009 1000 kg/mm^2, E = 210000 N/ mm2, and υ = 0.3. Shell elements SHELL163 were used, having a Belytschko-Tsay formulation and 3 integration points over

the thickness. For verification purposes, also implicit simulations, using the same model, were carried out. Results are shown in figure 5.

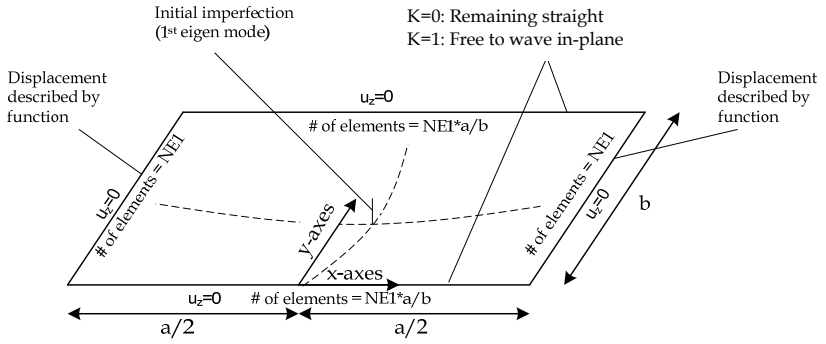

Figure 4, finite element model for explicit dynamic analyses of part of compressed flange

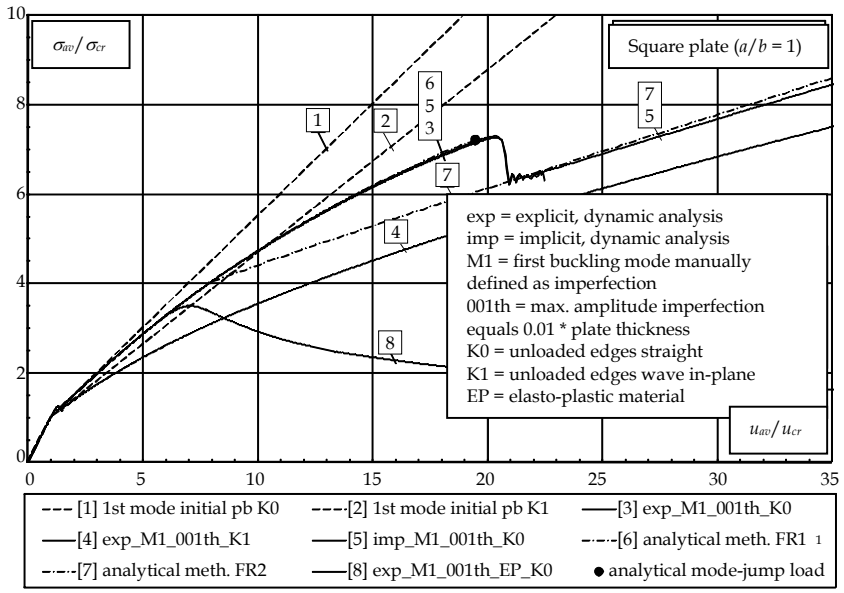

Figure 5, dimensionless stress-shortening behavior

In figure 5, all the results of the finite element simulations (curves 3,4,5,8) start with a manually defined imperfection, this to ensure an exact similar initial imperfection. Also, results from an analytical approximation method have been obtained (curves 1,2,6,7) [Cour11a]. These have no initial imperfection but the difference is negligible because the assumed imperfection in the finite element analyses is extremely small compared to the plate's thickness. Curves 1 and 2 represent the analytically approached initial post-buckling behavior of a plate with the unloaded edges remaining straight and free to wave in-plane respectively. Branches 2 and 3 represent the explicit finite element simulation results of a plate with the unloaded edges remaining straight and free to wave in-plane respectively also. Branch 5 is equal to branch 3, although now performed via an implicit analysis for verification purposes. Branches 6 and 7 represent the behavior obtained by the analytical approximation method using different displacement functions. Branch 8, finally is equal to branch 4, although now bilinear elasto-plastic material behavior is assumed, which is not relevant for this paper. Buckling can be seen around u_{av}/u_{cr} = 1.5 and analytical and finite element simulations show mode-jumping for u_{av}/u_{cr} = 21. However, mode-jumping is only seen for the cases where unloaded edges (those along the length) are forced to remain straight. The analytical method and finite element simulations show good correlation for all cases and thus the results obtained here seem to be trustworthy.

The square plate presented above may not be representative for a compressed flange of trapezoidal sheeting. Therefore, finite element simulations were carried out on long compressed plates for a/b=5, 10, and 14. Note that for these plates, the analytical model is not applicable, however, it was believed that a finite element model that was verified for a square plate should also be able to indicate the behavior for a non-square, long plate. Results are similar for the three a/b ratios selected and are shown in figure 6 for a/b=10, curve 3. After buckling the long plate shows 10 buckles, after mode-jumping (at u_{av}/u_{cr} = 9) 14 buckling show up, which changes into 20 buckles after a second mode-jump (at u_{av}/u_{cr} = 28).

An important conclusion that can be drawn from the finite element analyses (and the analytical method not presented here) is that for plates, both short and long, with longitudinal unloaded edges that are free to wave in-plane, mode-jumping does not occur. Based on this conclusion, it is highly unlikely that the phenomenon occurs in the compressed flange of trapezoidal sheeting that is subjected to a combination of a concentrated load and a bending moment as the unloaded edges of the compressed flanges are barely supported inwards by the webs. One may think that due to the fact that the webs usually join the flanges at an angle larger than 90 degrees, they supply some resistance to the flange

waving in-plane, however this effect is thought to be negligible. As such, the convergence problems experienced in the past (for simulating the yield-eye post-failure) are not likely to be caused by mode-jumping phenomena, especially because during the research presented above, even some implicit static simulations showed to be capable to cover some of mode jumping phenomena [Cour11a]. Furthermore, the fact that mode-jumping is not likely to occur, makes it unlikely that mode-jumping influences the post-failure mode that occurs (yield-arc or yield-eye).

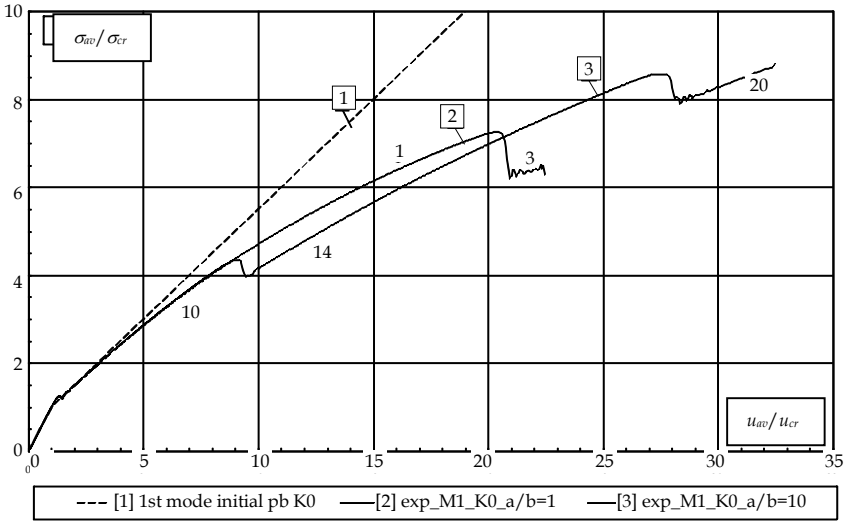

Figure 6, dimensionless stress-shortening behavior for a/b=10 (curve 3)

3 Full-size finite element model

As mentioned, in the past, using an implicit, static finite element model, convergence problems were experienced in modeling the yield-eye post failure mode. Although in the previous section it was shown that these convergence problems are not likely to be caused by mode-jumping phenomena, and thus that using an explicit, dynamic finite element method may not be a solution, in the research to be presented here nevertheless an explicit dynamic finite element model has been used. This because an explicit solving strategy may also help against other convergence problems, for instance those caused by contact problems. The principle of the finite element model is shown in figure 7.

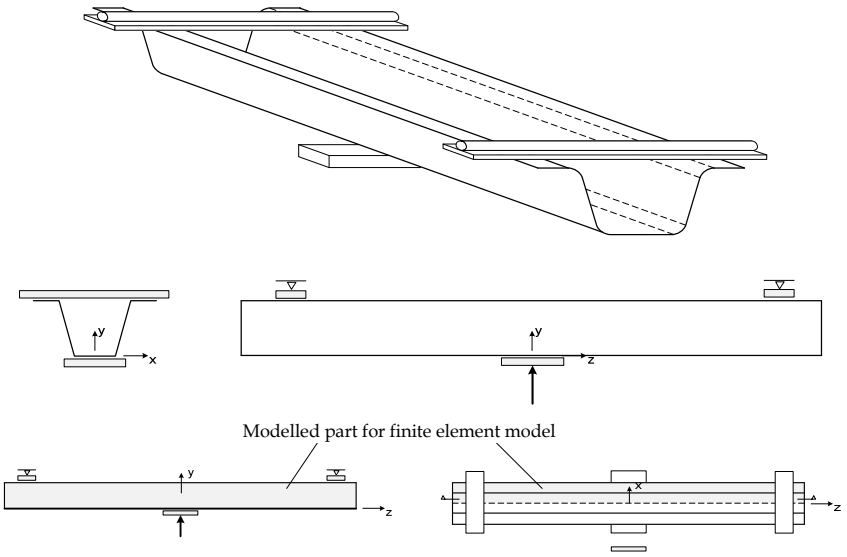

Figure 7, experiment at the top, modeled part for the finite element model at the bottom

As can be seen at the bottom of figure 7, the finite element simulation models a half sheet-section, this because a quarter model, which would be more efficient, would not enable the asymmetric yield-eye post-failure mode to occur. Four node shell elements (SHELL163) are used to model the sheet-section and a fine mesh is used near the load bearing plate. This fine mesh is coupled via a transition mesh to the more course meshed outer parts of the section. The corner radii are modeled using several elements along the circumference. The hinge supports, as shown in figure 7, are modeled by applying boundary conditions to the nodes at the hinge supports as follows: fixed in *x*- and *y*-direction and for rotation around the *y*- and *z*-axes, free in *z*-direction and for rotation around the *x*-axes. In the experiments several steel strips were fixed between the upper flange parts (the flange parts under tension) to avoid spreading of the webs. These strips have been modeled by fixing the nodes at the strips in *x*-direction. The load bearing plate was modeled by a rigid volume and the contact between the load bearing plate and the section was modeled explicitly. The steel material was modeled using test coupon data in a piecewise linear plasticity model. For this a strain rate dependency was not used as a quasi-static analysis was carried out. More details on the finite element model can be found in [Cour11a].

Two parameter studies have been carried out with the finite element model above. First of all, the influence has been investigated of relevant finite element model related parameters, i.e. imperfection size, solver precision, type of top flange support, damping, load type, number of corner elements, and amount of friction between the load bearing plate and sheet-section on general behavior. Secondly, a parameter study has been undertaken to investigate the effect of sheet-section properties and those are the span length, top flange width, web width, bottom flange width, angle between web and flange, corner radius, imperfection (again), number of corner elements, and strips against sway. Both parameter studies will be presented briefly below.

4 Parameter study for finite element model

The first parameter study is shown in table 1, with simulation TSSv23_1 (second row) being the reference simulation.

Table 1, geometry and model parameters first study

TSS v23	L_{span} [mm]	θ_w [deg]	r_{bf} [mm]	b_{bf} [mm]	*eccent* [mm]	*lct*	*hct*	*strp*	*msf*	*NErb*	mech
0	As **1** but without mass scaling										**A**
1	2400	50	5	40	0	1	0	1	2	2	**A**
1a	As **1** but with single precision										**A**
1b	As **1** but with load-bearing plate nodes aligned with sheeting nodes										**A**
1c	As **1** but with full top flange support (no strips)										**A**
1d	As **1** but with alpha damping (after 12mm displacement of load-bearing plate)										**A**
1e	As **1** but with *lct*=2 (constant acceleration)										**A**
1f	As **1** but with 4 elements modeled in the corner (instead of 2)										**A**
3	2400	50	5	40	2.5	1	0	1	2	2	**E**
3a	As **3** but with friction (0.7 static friction coefficient)										**E**
3b	As **3** but with friction (0.15 static friction coefficient)										**E**
3c	As **3a** but with full top flange support (no strips)										**E**
4	2400	70	5	40	*	1	0	1	2	2	**E**
	* eccentricity due to smaller thickness at one side of load-bearing plate										

Mass scaling is a technique in which the (mass) density of a structure is increased, which results in a larger minimum required time step during explicit simulations, thus reducing the total simulation time. However, modifying the mass influences the dynamic behavior and is thus only suitable for quasi-static simulations in which the kinetic energy (=external work minus strain energy) is low. Compared against a simulation without mass scaling (TSSv23_0, first row), the reference simulation shows that mass scaling decreases simulation time with a factor 3, however influences the correctness of the simulations with only 2 percent. Simulation TSSv23_1a shows that single precision seems to yield the

same post-failure mode (yield-arc) as the reference simulation, however if nodal displacements are studied in more detail, differences in symmetry can be found for the single precision case (in the order of number accuracy), which may trigger a yield-eye post-failure mode. Therefore double precision should be used. A similar issue can be seen if load-bearing plate nodes are aligned exactly at nodes of the sheeting (TSSv23_1b). Also in this case some small differences in nodal displacements occur, such that symmetry is not completely fulfilled. If nodes of the load bearing plate are halfway between the sheeting nodes, as in the reference case, this goes without problems. Whether discrete strips or continuous boundary conditions along the length of the top flange are modeled proofs not to make any difference in sheeting behavior, both for the yield arc post-failure mode (shown by simulation 1c) and for the yield-eye mode (shown in the following section). Regarding the load application, alpha damping (simulation 1d) and constant acceleration (simulation 1e) do not change the post-failure mode to occur, however, do not improve the reference simulations with respect to load fluctuations after ultimate load, and as such, they are not used for further simulations. This is also the case for using 4 instead of 2 elements in the corner (simulation 1f). Simulations 3, 3a to c, and 4 show that introducing an imperfection, regardless due to a load bearing plate eccentricity or a smaller thickness of the sheeting at one location, a yield-eye post-failure mode occurs, as shown in figure 8.

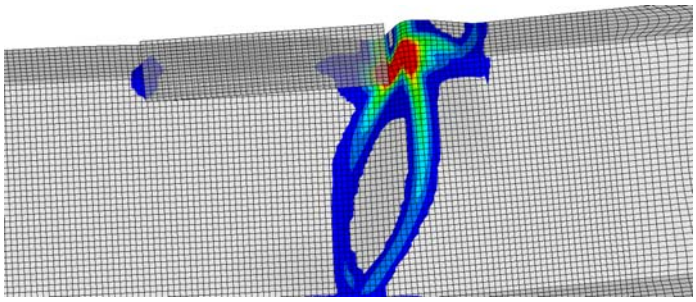

Figure 8, yield-eye post-failure mode

5 Parameter study for post-failure modes

To understand under which conditions a certain post-failure mode occurs (i.e. a yield-arc or a yield-eye post-failure mode), the finite element model as investigated in the previous section (the reference model TSSv23_1) is now used for the simulation of specific experiments carried out in the past [Hofm02a]. These simulations can be seen as a parameter study for which

sheeting properties are varied that also vary normally in practical applications, table 2. For every case, the table also lists the post-failure mode and ultimate load as they were observed during the experiments.

Table 2, geometry and model parameters first study

Experiment number [#]

			r_{bf}	1	5
			L_{lb}	100	100
L_{span}	θ_w	b_{bf}			
1800	90	100			**46**
	70	100			**48**
	50	40		**42**	
2400	90	100			**58**
	50	40		**54**	**63**

Post-failure mode [A/E]

			r_{bf}	1	5
			L_{lb}	100	100
L_{span}	θ_w	b_{bf}			
1800	90	100			**A**
	70	100			**A**
	50	40		**A**	
2400	90	100			**A**
	50	40		**E**	**E**

Ultimate load [N]

			r_{bf}	1	5
			L_{lb}	100	100
L_{span}	θ_w	b_{bf}			
1800	90	100			**2768**
	70	100			**2630**
	50	40		**2388**	
2400	90	100			**2169**
	50	40		**2572**	**1756**

All the experiments in table 2 were simulated twice: once with modeled strips preventing spreading of the webs (thus simulating exactly the sheet-section experiments) and once with continuous boundary conditions along the top flange edge (this situation models sheeting). All experiments were given a 2.5 mm load bearing plate eccentricity to provoke a possible yield-eye post failure mode. For experiment 58 and 63, an additional imperfection equal to 5 mm was tried as well.

For the simulations, both the ultimate load and the occurring post-failure modes correspond accurately to the experiments. One exception however, the post-failure mode of experiment 63 is predicted by the simulation to be a (symmetric) yield-arc post-failure mode in the case of 2.5 mm eccentricity. For a double 5 mm eccentricity, the correct (asymmetric) yield-eye post-failure mode is simulated. This indicates that to simulate a yield-eye post-failure mode, the (single) imperfection should be selected large enough, even if this imperfection is not expected to be present with this magnitude in the experiment. This seems to be acceptable, as in the experiment it is possible that several smaller imperfections (material properties, out-of-plane deflections, etc.) add up to an effect that can be compared with a slightly larger single imperfection in the finite element model. Now it may be questioned whether a double eccentricity may result in other analyses, which first showed a yield-arc post-failure mode, now showing a yield-eye post-failure mode (while the experiment shows a yield-arc). This has been examined by applying a double eccentricity to the

simulation of experiment 58, but here still a yield-arc is found. This leads to the conclusion that the size of the eccentricities is very important because when chosen too small, a yield-arc will be found although the yield-eye should be found. The other way around, applying a larger eccentricity to a sheet section that should yield a yield-arc (according to the experiments) does not lead to a yield-eye post-failure mode. So sections with properties that lead to a yield-eye in the experiments are more sensitive to eccentricities (and imperfections). Finally, no differences were found for the simulations with strips preventing spreading of the webs or those with continuous boundary conditions along the top flange edge (corresponding to sheeting in practice).

6 Prediction of the occurring post-failure mode

During experiments and simulations, the observed behavior of the two post-failure modes suggest that a ratio between the concentrated load, which deforms the cross-section locally, and the bending moment in the sheet-section, which causes an (elasto-plastic) shortening of the compressed flange, may predict the occurrence of either the yield-arc or yield-eye post-failure mode. Namely, the yield-arc post-failure mode shows severe cross-sectional deformations, presumably caused by the concentrated load, whereas the yield-eye post-failure shows a clear shortening of the compressed flange, probably caused by the bending moment, which in turn is caused by the concentrated load and span length of the sheet-section. To investigate the usefulness of the suggested ratio, stress ratios have been determined for all finite element simulations as shown in figure 9. The membrane stress in the compressed (bottom) flange in length direction is divided by the membrane stress in height direction in the web.

If the ratios determined as suggested above are plotted with the post-failure mode indicated, it is shown that for low ratios indeed the yield-eye post failure mode occurs whereas for high ratios a yield-arc is present. An exception is simulation TSSv23a63exp.1a, but is was explained in the previous section that for this simulation the eccentricity was too small and consequently it should not be taken into account here. However, it has been shown that the suggested ratio is dependent on the mesh size and additional research should be carried out to solve this problem.

Conclusions

This paper presents research on sheeting, in which both the compressed flange in isolation and the full sheet-section is modeled by using an explicit, dynamic finite element model.

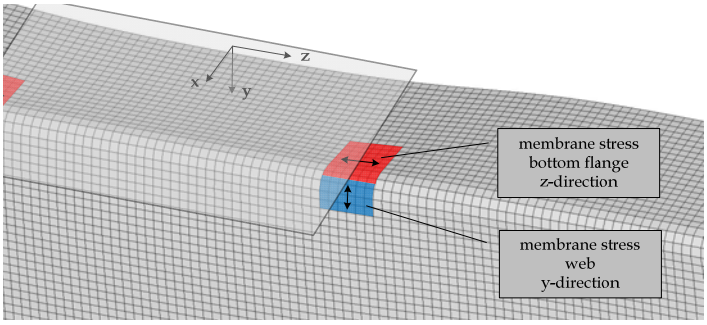

Figure 9, ratio between membrane stress in web (due to concentrated load) and membrane stress in (compressed) bottom flange

It is indicated that mode-jumping phenomena are not likely to occur for trapezoidal sheeting as used in practice.

For a sheet-section for which a yield-eye post-failure mode may occur (potentially), the imperfection size is the most determining factor whether the yield-arc or yield-eye post-failure mode occurs.

A simple yet accurate prediction formula has been derived, which predicts the mode occurring, thus enabling future investigations into the sheeting's behavior, like moment redistribution and behavior for second and third generation sheeting.

Acknowledgements

M.Sc.-student J. Courage carried out the research as presented in this paper. His work is highly appreciated and was also rewarded last year by the Dutch national first prize "StudentenSTAALprijs 2011". Besides by the author, he was also supervised by Full Professor Dr. J.G.M. Kerstens, and Full Professor F. Soetens. Their help is highly appreciated as well.

Appendix.-References

[Akha04a] Akhand, A.M.; Wan Badaruzzaman, W.H.; Wright H.D.: Combined flexure and web crippling strength of a low-ductility high strength steel decking: experiment and a finite element model, Thin-Walled Structures, Volume 42, Issue 7, July 2004, Pages 1067-1082.

[Ansy11a] Ansys 12.1, ANSYS, Inc., Southpointe, 275 Technology Drive, Canonsburg, PA 15317, United States of America.
[Bakk06a] Bakker, M.C.M.; Rosmanit, M.; Hofmeyer, H.: Elastic post-buckling behaviour of uniformly compressed plates, LaBoube, Roger A.; Yu, Wei-Wen: Proceedings 18th International Speciality Conference on Recent Research and Developments in Cold-Formed Steel Design and Construction, October 26 & 27, 2006, Orlando, Florida, U.S.A, Department of Civil, Architectural & Environmental Engineering, University of Missouri-Rolla, Rolla, Missouri, page 1-15.
[Beda09a] Bedair, O.: Stability of web plates in W-shape columns accounting for flange/web interaction, Thin-Walled Structures, Volume 47, Issue 6-7, June 2009, Pages 768-775
[Beda10a] Bedair, O.: Stability analysis of plates with partial restraints using unconstrained optimization techniques, International Journal of Structural Stability and Dynamics, Volume 10, Issue 3, September 2010, Pages 571-587.
[Beda11a] Bedair, O.: Graphical representation for stability limit state design of wide flange beam-column I-sections, Recent Patents on Engineering, Volume 5, Issue 3, December 2011, Pages 190-195.
[Bieg06a] Biegus, A.; Czepiżak, D.: Research on the interactive resistance of corrugated sheets under combined bending and contact pressure, Thin-Walled Structures, Volume 44, Issue 8, August 2006, Pages 825-831.
[Bieg08a] Biegus, A.; Czepizak, D.: Experimental investigations on combined resistance of corrugated sheets with strengthened cross-sections under bending and concentrated load, Thin-Walled Structures, Volume 46, Issue 3, March 2008, Pages 303-309.
[Chen12a] Chen, D.H.: The collapse mechanism of corrugated cross section beams subjected to three-point bending, Thin-Walled Structures, Volume 51, February 2012, Pages 82-86.
[Cour11a] Courage, J.; Hofmeyer, H.; Kerstens, J.G.M.; Soetens, F.: Research Report: Failure Mechanisms of Thin-Walled Trapezoidal Steel Sheeting, M.Sc.-thesis, Eindhoven University of Technology, Department of the Built Environment, Structural Design Group, The Netherlands.
[Debo09a] Debowski, D.; Magnucki, K.; Malinowski, M.: Dynamic stability of a metal foam rectangular plate, Steel and Composite Structures, Volume 10, Issue 2, April 2010, Pages 151-168.
[Guze06a] Guzelbey, I.H.; Cevik, A.; Erklig, A.: Prediction of web crippling strength of cold-formed steel sheetings using neural networks, Journal of Constructional Steel Research, Volume 62, Issue 10, October 2006, Pages 962-973.
[Heda08a] Hedaoo, N.A.; Gupta, L.M.; Ronghe, G.N.; Parikh, S.K.: State of the art report on thin-walled cold-formed profiled steel decking, Proceedings 19th International Specialty Conference on Recent Research and Developments in

Cold-Formed Steel Design and Construction 2008, St. Louis, MO, Pages 307-323.
[Hofm02a] Hofmeyer, H.; Kerstens, J.G.M.; Snijder, H.H.; Bakker, M.C.M.: Combined Web Crippling and Bending Moment Failure of First-Generation Trapezoidal Steel Sheeting, Journal of Constructional Steel Research, Volume 58, Number 12, page 1509-1529, ISSN 0143-974X, 2002.
[Lang06a] Langdon, G.S.; Schleyer, G.K.: Deformation and failure of profiled stainless steel blast wall panels. Part III: Finite element simulations and overall summary, International Journal of Impact Engineering , Volume 32, Issue 6, June 2006, Pages 988-1012
[Macd06a] Macdonald, M.; Heiyantuduwa, M.A.; Rhodes, J.: Finite element analysis of web crippling behaviour of cold-formed steel flexural members, Proceedings 18th International Specialty Conference on Cold-Formed Steel Structures: Recent Research and Developments in Cold-Formed Steel Design and Construction, Orlando, FL.
[MacD11a] MacDonald, M.; Heiyantuduwa, M.A.: A design rule for web crippling of cold-formed steel lipped channel beams based on nonlinear FEA, Thin-Walled Structures, Volume 53, April 2012, Pages 123-130.
[MacD11b] MacDonald, M.; Heiyantuduwa Don, M.A.; Kotełko, M.; Rhodes, J.: Web crippling behaviour of thin-walled lipped channel beams, Thin-Walled Structures, Volume 49, Issue 5, May 2011, Pages 682-690.
[Marg38a] Marguerre, K.: Zur Theorie der gekrümmter Platte grosser Formänderung, Proc. Fifth. Int. Congress Appl. Mech., Page 93, 1938.
[Than11a] Thanga, T.; Halabiah, B.; Sivakumaran, K.S.: Strength of plates of rectangular industrial ducts, Procedia Engineering, Volume 14, 2011, Pages 622-629.
[Tsew08a] Tse, W.T.; Chung, K.F.: Web crippling behaviour of laterally restrained cold-formed steel re-entrant profiled deckings, Journal of Constructional Steel Research, Volume 64, Issue 7-8, July 2008, Pages 785-801.
[Zhou07a] Zhou, F.; Young, B.: Experimental and numerical investigations of cold-formed stainless steel tubular sections subjected to concentrated bearing load, Journal of Constructional Steel Research, Volume 63, Issue 11, November 2007, Pages 1452-1466.

Appendix.-Notation

F	(Concentrated) load (figure 1)
L_{lb}	Load bearing plate width (figure 1, table 2)
x,y,z	coordinate axes (figure 2)
u,v,w	displacements according coordinate axes x,y,z (figure 2)
NE1	Number of elements, variable 1 [1] (figure 3)
a	Plate length (figure 3)

b	Plate width (figure 3)
u_z	Out-of-plane plate deformation (figure 3)
ρ	Density [kg/mm^2]
E	Young's modulus [N/mm^2]
υ	Poisson's ratio [1]
σ_{cr}	Buckling stress (figure 5)
σ_{av}	Average stress (figure 5)
u_{cr}	Controlled displacement at buckling (figure 5)
u_{av}	Controlled average displacement (figure 5)
K	Edge b.c.: "0" = straight, "1" = wave in-plane (figure 4)
L_{span}	Span length [mm] (figure 1, table 1,2)
θ_w	Angle between web and flange [deg.] (table 1,2)
r_{bf}	Radius of compressed flange corner [mm] (table 1,2)
b_{bf}	Bottom flange width [mm] (table 1,2)
eccent	Eccentricity load bearing plate in length direction [mm] (table 1)
lct	Loading, "1" = via constant speed, "2" = via constant acceleration (table 1)
hct	Load bearing plate friction, "0" = no, "1" = yes (table 1)
strp	Preventing spreading of the webs, "1" = strips, "2" = continuous support (table 1)
msf	mass scaling factor [1] (table 1)
NErb	Number of elements [1] (table 1)
mech	Post-failure mode: "A" = yield-arc, "E" = yield-eye (table 1)